Influence of the Lattice Parameter Difference between the Two Cubic Phases Formed in the 4 V Region on the Capacity Fading of Spinel Manganese Oxides

Youngjoon Shin and A. Manthiram*

Materials Science and Engineering Program, The University of Texas at Austin, Austin, Texas 78712

Received March 19, 2003. Revised Manuscript Received May 19, 2003

To develop a better understanding of the capacity-fading mechanisms of spinel lithium manganese oxides, the electrochemical properties, degree of manganese dissolution, and crystal chemistry of a number of singly substituted $LiMn_{2-y}M_yO_4$ (M = Li, Al, Ti, Co, and Ni and $0 \le y \le 0.2$) and doubly substituted $LiMn_{2-y-z}M_yLi_zO_4$ (M = Ti, Co, and Ni, $0 \le y \le 0.1$, and $0 \le z \le 0.1$) oxides have been compared with those of $LiMn_2O_4$. The cation-substituted spinel manganese oxides show better electrochemical performances than $LiMn_2O_4$. Especially, the doubly substituted $LiMn_{1.85}Ni_{0.075}Li_{0.075}O_4$ exhibits excellent cyclability at both ambient and elevated temperatures with a capacity of around 100 mAh/g. It also exhibits remarkable rate capability and excellent capacity retention (>95%) after storage at 60 °C at various depths of discharge (DOD). Although the degree of manganese dissolution does not vary significantly, the spinel manganese oxides show a clear relationship between the percent capacity fade and the lattice parameter difference (Δa) between the two cubic phases formed in the 4 V region. A smaller Δa and the associated negligible volume change (ΔV) appear to minimize the microstrain, maintain good interparticle contact, and lead to superior electrochemical performances. The excellent cyclability and high rate capability of the $LiMn_{2-y-z}Ni_yLi_zO_4$ oxides may make them attractive for electric vehicles.

Introduction

Lithium-ion batteries have become attractive for portable electronic devices because of their higher energy density compared to that of other rechargeable systems, and they are being intensively pursued for electric vehicle applications. Commercial lithium-ion cells currently use layered $LiCoO_2$ cathodes, but Co is expensive and relatively toxic. These drawbacks have prompted the development of alternative cathodes, especially for electric vehicle applications. In this regard, $LiMn_2O_4$ crystallizing in the spinel structure has become appealing as Mn is inexpensive and environmentally benign. However, the spinel $LiMn_2O_4$ oxide is confronted with capacity fade particularly at elevated temperatures. Several mechanisms have been proposed in the literature to account for the capacity fade: (1) formation of tetragonal $Li_2Mn_2O_4$ on the surface of $LiMn_2O_4$ and the associated lattice (Jahn−Teller) distortion,[1] (2) manganese dissolution into the electrolyte,[2−9] (3) oxygen defects,[10] (4) formation of new phases,[11] (5) loss of crystallinity,[12,13] (6) instability arising from the existence of two cubic phases,[14,15] and (7) development of microstrain[16] during cycling. Among them, manganese dissolution is generally thought to be the most important factor, but it has been shown to account for only some portion of the total capacity loss.[3,5,14] Also, recent characterization of chemically delithiated $Li_{1-x}Mn_2O_4$ samples has shown that they do not experience any oxygen loss from the lattice[17] during charge, contrary to some speculative reports in the literature.

Several strategies have been pursued over the years to suppress the capacity fade experienced by the spinel

* To whom correspondence should be addressed. Tel: 512-471-1504. Fax: 512-471-7681. E-mail: rmanth@mail.utexas.edu.

(1) Thackeray, M. M.; Shao-Horn, Y.; Kahaian, A. J.; Kepler, K. D.; Skinner, E.; Vaughey, J. T.; Hackney, S. A. *Electrochem. Solid-State Lett.* **1998**, *1*, 7.
(2) Jang, D. H.; Shin, Y. J.; Oh, S. M. *J. Electrochem. Soc.* **1996**, *143*, 2204.
(3) Xia, Y.; Zhou, Y.; Yoshio, M. *J. Electrochem. Soc.* **1997**, *144*, 2593.
(4) Inoue, T.; Sano, M. *J. Electrochem. Soc.* **1998**, *145*, 3704.
(5) Yamane, H.; Inoue, T.; Fujita, M.; Sano, M. *J. Power Sources* **2001**, *99*, 60.
(6) Aoshima, T.; Okahara, K.; Kiyohara, C.; Shizuka, K. *J. Power Sources* **2001**, *97−98*, 377.
(7) Park, S.-C.; Han, Y.-S.; Kang, Y.-S.; Lee, P. S.; Ahn, S.; Lee, H.-M.; Lee, J.-Y. *J. Electrochem. Soc.* **2001**, *148*, A680.
(8) Liu, Z.; Wang, H.; Fang, L.; Lee, J. Y.; Gam, L. M. *J. Power Sources* **2002**, *104*, 101.
(9) Komaba, S.; Kumagai, N.; Sasaki, T.; Miki, Y. *Electrochemistry* **2001**, *69*, 787.
(10) Wang, X.; Nakamura, H.; Yoshio, M. *J. Power Sources* **2002**, *110*, 19.
(11) Palacin, M. R.; Chabre, Y.; Dupont, L.; Hervieu, M.; Strobel, P.; Rousse, G.; Masquelier, C.; Anne, M.; Amatucci, G. G.; Tarascon, J. M. *J. Electrochem. Soc.* **2000**, *147*, 845.
(12) Huang, H.; Vincent, C. A.; Bruce, P. G. *J. Electrochem. Soc.* **1999**, *146*, 3649.
(13) Aurbach, D.; Levi, M. D.; Gamulski, K.; Markovsky, B.; Salitra, G.; Levi, E.; Heider, U.; Heider, L.; Oesten, R. *J. Power Sources* **1999**, *81*, 472.
(14) Lee, J. H.; Hong, J. K.; Jang, D. H.; Sun, Y.-K.; Oh, S. M. *J. Power Sources* **2000**, *89*, 7.
(15) Xia, Y.; Yoshio, M. *J. Power Sources* **1997**, *66*, 129.
(16) Shin, Y.; Manthiram, A. *Electrochem. Solid-State Lett.* **2002**, *5*, A55.
(17) Chebiam, R. V.; Kannan, A. M.; Prado, F.; Manthiram, A. *Electrochem. Commun.* **2001**, *3*, 624.

10.1021/cm0341787 CCC: $25.00
Published on Web 06/13/2003

Table 1. Electrochemical and Crystal-Chemical Data of Spinel Manganese Oxides

sample number	composition	initial capacity (mAh/g)	% capacity loss after 50 cycles at 25 °C	calculated Mn valence[a]	lattice parameter (Å)	% volume change in the two-phase region
1	$LiMn_2O_4$	118.6	39.4	3.50	8.2489	2.99
2	$LiMn_{1.95}Li_{0.05}O_4$	121.4	9.6	3.56	8.2319	1.17
3	$LiMn_{1.9}Li_{0.1}O_4$	108.6	4.2	3.63	8.2179	0.48
4	$LiMn_{1.9}Co_{0.1}O_4$	123.2	14.9	3.53	8.2319	2.58
5	$LiMn_{1.8}Co_{0.2}O_4$	109.3	5.5	3.56	8.2103	
6	$LiMn_{1.9}Ni_{0.1}O_4$	119.9	9.6	3.58	8.2319	2.08
7	$LiMn_{1.85}Ni_{0.15}O_4$	105.0	4.9	3.62	8.2086	
8	$LiMn_{1.8}Ni_{0.2}O_4$	92.4	3.6	3.67	8.2139	
9	$LiMn_{1.9}Al_{0.1}O_4$	116.8	28.4	3.53	8.2411	
10	$LiMn_{1.9}Ti_{0.1}O_4$	108.8	17.1	3.47	8.2493	
11	$LiMn_{1.9}Co_{0.05}Li_{0.05}O_4$	118.2	4.3	3.58	8.2212	0.54
12	$LiMn_{1.8}Co_{0.1}Li_{0.1}O_4$	97.1	1.2	3.67	8.2013	
13	$LiMn_{1.9}Ni_{0.05}Li_{0.05}O_4$	114.0	3.2	3.61	8.2181	0.53
14	$LiMn_{1.88}Ni_{0.06}Li_{0.06}O_4$	104.9	2.0	3.63	8.2138	
15	$LiMn_{1.85}Ni_{0.075}Li_{0.075}O_4$	95.3	0.9	3.66	8.2080	0.34
16	$LiMn_{1.8}Ni_{0.1}Li_{0.1}O_4$	82.7	0.5	3.72	8.2023	0.12
17	$LiMn_{1.9}Al_{0.05}Ti_{0.05}O_4$	113.3	25.1	3.55	8.2401	
18	$LiMn_{1.85}Ti_{0.075}Li_{0.075}O_4$	110.4	20.7	3.58	8.2305	2.17

[a] Calculated by assuming Al^{3+}, Co^{3+}, Ni^{2+}, and Ti^{4+}.

manganese oxides. For example, substitution of other cations for manganese in $LiMn_{2-y}M_yO_4$ (M = Li, Mg, Al Cr, Co, and Ni),[5,12−16,18−20] surface modification with other oxides,[7,8,21] and incorporation of additives into the electrolytes[22] have been shown to improve the capacity retention. However, the reasons for the improved capacity retention are not fully understood. We showed recently that a cosubstitution of small amounts of both Li and Ni for Mn in $LiMn_{2-2y}Ni_yLi_yO_4$ offers excellent capacity retention at elevated temperatures with remarkably high rate capability.[23] We present here a more systematic investigation and comparison of some singly substituted $LiMn_{2-y}M_yO_4$ (M = Li, Al, Ti, Co, and Ni and $0 \le y \le 0.2$) and doubly substituted $LiMn_{2-y-z}M_yLi_zO_4$ (M = Ti, Co, and Ni, $0 \le y \le 0.1$, and $0 \le z \le 0.1$) spinel oxides to develop a better understanding of the reasons for the improved capacity retention. The results indicate that the lattice parameter difference between the two cubic phases formed in the 4 V region and the consequent lattice strain play a critical role in the capacity fade of spinel manganese oxides.

Experimental Section

The $LiMn_{2-y}M_yO_4$ (M = Li, Al, Ti, Co, and Ni and $0 \le y \le 0.2$) and $LiMn_{2-y-z}M_yLi_zO_4$ (M = Ti, Co, and Ni, $0 \le y \le 0.1$, and $0 \le z \le 0.1$) samples were synthesized by solid-state reactions of Li_2CO_3 and Mn_2O_3 with Al_2O_3, TiO_2, Co_3O_4, or NiO at 800 °C for 48 h in air. All samples were characterized by X-ray powder diffraction to be single-phase materials, and the lattice parameters are given in Table 1. The lithium contents in the samples determined by atomic absorption spectroscopy were found to be similar to those in the starting reaction mixtures indicating negligible volatilization of lithium during the firing process. The electrochemical performance of the $LiMn_{2-y}M_yO_4$ and $LiMn_{2-y-z}M_yLi_zO_4$ cathodes were evaluated with CR2032 coin cells using metallic lithium anode and 1 M $LiPF_6$ in ethylene carbonate (EC) and diethyl carbonate (DEC) electrolyte. The cathodes were fabricated by mixing 75 wt % $LiMn_{2-y-z}M_yLi_zO_4$ with 20 wt % acetylene black and 5 wt % of poly(tetrafluoroethylene) (PTFE) binder, rolling the mixture into thin sheets of about 0.2 mm thick, and cutting into circular electrodes of 0.65 cm^2 area. Electrochemical data were collected between 4.3 and 3.5 V at various rates between C/10 and 20C at room temperature and 60 °C. Cyclic voltammogram (CV) plots were recorded between 3.6 and 4.3 V at a scan rate of 50 μV/s.

The degree of manganese dissolution was assessed by (1) soaking the $LiMn_{2-y-z}M_yLi_zO_4$ powder for 7 days at 55 °C in the electrolyte consisting of 1 M $LiPF_6$ in ethylene carbonate (EC) and diethyl carbonate (DEC) and (2) washing the coin cell components (cathode, anode, and separator) with deionized water or propylene carbonate at room temperature after cycling at 60 °C for 20 cycles, followed by analyzing the manganese content by atomic absorption spectroscopy (AAS).

Chemical extraction of lithium was carried out by stirring the $LiMn_{2-y-z}M_yLi_zO_4$ powder either with 2.5 N sulfuric acid[24] at room temperature for 1 h followed by washing the products with water, or with an acetonitrile solution of the oxidizing agent NO_2BF_4 at room temperature for 2 days under argon atmosphere using a Schlenk line followed by washing the products with acetonitrile.[17,25] The $Li_{1-x}Mn_{2-y-z}M_yLi_zO_4$ samples obtained by both the methods, as well as those obtained after soaking with the electrolytes, were used for strain analysis, but only the samples obtained with NO_2BF_4 were used for monitoring the lattice parameter variation with lithium content. The grain size and strain analyses were made with X-ray diffraction data using the JADE software.[16] Lattice parameter determinations were made by Rietveld analysis with the DBWS-9411 PC program.[26] The lithium contents in $Li_{1-x}Mn_{2-y-z}M_yLi_zO_4$ were determined by atomic absorption spectroscopy.

Results and Discussions

Cycling Performance. Figures 1 and 2 compare the cyclability data of the $LiMn_{2-y-z}M_yLi_zO_4$ and $LiMn_{2-y-z}M_yLi_zO_4$ samples at room temperature and 60 °C, respectively. The initial capacity values and the %

(18) Robertson, A. D.; Lu, S. H.; Howard, W. F., Jr. *J. Electrochem. Soc.* **1997**, *144*, 3505.
(19) Hong, Y.-S.; Han, C.-H.; Kim, K.; Kwon, C.-W.; Campet, G.; Choy, J.-H. *Solid State Ionics* **2001**, *139*, 75.
(20) Gummow, R. J.; De Kock, A.; Thackeray, M. M. *Solid State Ionics* **1997**, *69*, 59.
(21) Kannan, A. M.; Manthiram, A. *Electrochem. Solid-State Lett.* **2002**, *5*, A167.
(22) Sun, X.; Lee, H. S.; Yang, X. Q.; McBreen, J. *Electrochem. Solid-State Lett.* **2001**, *4*, A184.
(23) Shin, Y.; Manthiram, A. *Electrochem. Solid-State Lett.* **2003**, *6*, A34.
(24) Hunter, J. C. *J. Solid State Chem.* **1981**, *39*, 142.
(25) Chebiam, R. V.; Prado, F.; Manthiram, A. *Chem. Mater.* **2001**, *13*, 2951.
(26) Young, R. A.; Shakthivel, A.; Moss, T. S.; Paiva Santos, C. O. *J. Appl. Crystallogr.* **1995**, *28*, 366.

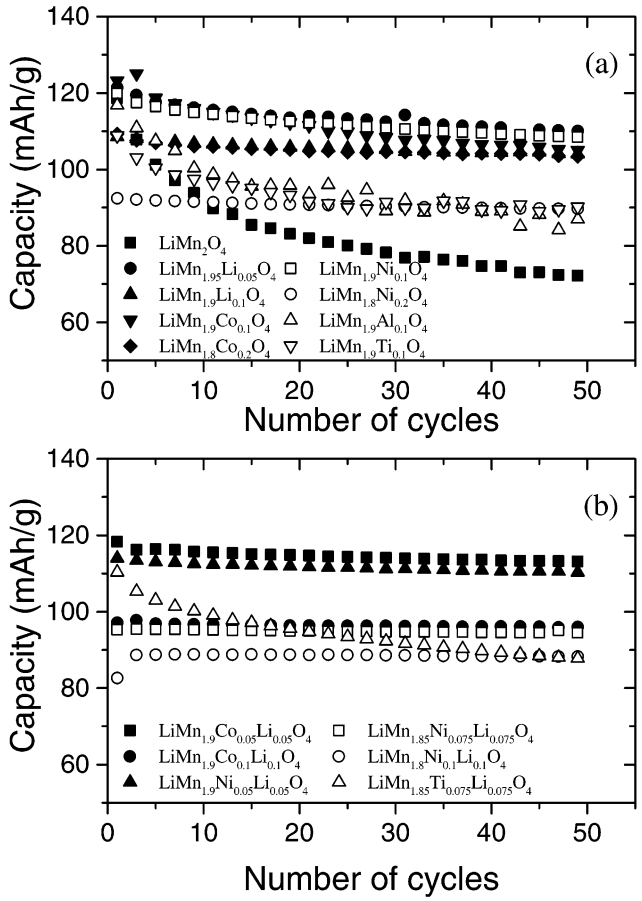

Figure 1. Comparison of the cycling performances of (a) singly substituted and (b) doubly substituted spinel manganese oxides with that of $LiMn_2O_4$ at C/5 rate (~0.2 mA/cm^2) between 4.3 and 3.5 V at room temperature.

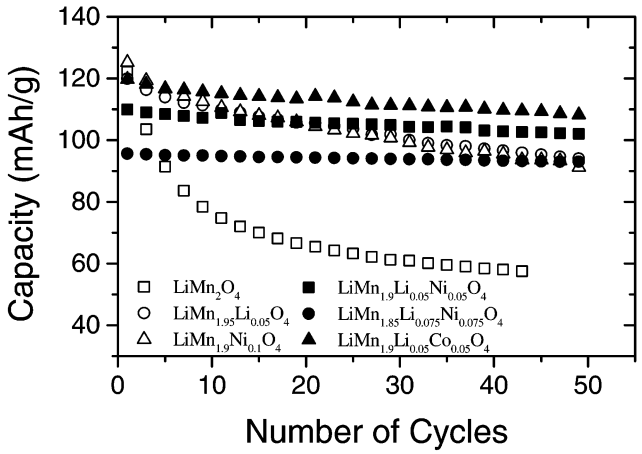

Figure 2. Comparison of the cycling performances of singly and doubly substituted spinel manganese oxides with that of $LiMn_2O_4$ at C/5 rate (~0.2 mA/cm^2) between 4.3 and 3.5 V at 60 °C.

capacity loss after 50 cycles at room temperature are summarized in Table 1. All the cation-substituted samples show much better capacity retention than the unsubstituted $LiMn_2O_4$ although some of them exhibit lower capacities, as has been found before by several groups.[12−16,18−20,23] The cation-substituted samples have an average oxidation state of >3.5+ for Mn, excepting $LiMn_{1.9}Ti_{0.1}O_4$, and one may argue that the improved cyclability could be due to the increased manganese valence and the consequent suppression of Jahn−Teller distortion. However, the data in Table 1 do not exhibit a systematic or linear variation of the % capacity loss with the oxidation state of Mn. For example, $LiMn_{1.9}Ni_{0.1}O_4$, $LiMn_{1.9}Co_{0.05}Li_{0.05}O_4$, and $LiMn_{1.85}Ti_{0.075}Li_{0.075}O_4$ have the same oxidation state of 3.58+ for Mn, but differ significantly in their % capacity loss (4.3−20.7%). Also, $LiMn_{1.9}Ti_{0.1}O_4$ with a lower oxidation state of 3.47+ for Mn exhibits better capacity retention than $LiMn_{1.9}Al_{0.1}O_4$, $LiMn_{1.9}Al_{0.05}Ti_{0.05}O_4$, and $LiMn_{1.85}Ti_{0.075}Li_{0.075}O_4$ withan oxidation state of >3.5+.

Table 1 also shows that for the same degree of cationic substitution, some of the doubly substituted samples exhibit better capacity retention than the singly substituted samples. For example, $LiMn_{1.9}Ni_{0.05}Li_{0.05}O_4$, $LiMn_{1.85}Ni_{0.075}Li_{0.075}O_4$, and $LiMn_{1.8}Ni_{0.1}Li_{0.1}O_4$ exhibit lower capacity loss (3.2−0.5%) than $LiMn_{1.9}Ni_{0.1}O_4$, $LiMn_{1.85}Ni_{0.15}O_4$, and $LiMn_{1.8}Ni_{0.2}O_4$ (9.6−3.6%). Similarly, $LiMn_{1.9}Co_{0.05}Li_{0.05}O_4$ and $LiMn_{1.8}Co_{0.1}Li_{0.1}O_4$ exhibit lower capacity loss (4.3−1.2%) than $LiMn_{1.9}Co_{0.1}O_4$ and $LiMn_{1.8}Co_{0.2}O_4$ (14.9−5.5%). These differences are difficult to explain based on the increased oxidation state of Mn and the suppression of Jahn−Teller distortion alone. Clearly, other factors appear to play a role.

Rate Capability. Rate capabilities of some selected spinel oxides were investigated by charging at the same rate of C/5 and discharging at different rates of C/10, C/5, C/2, 1C, 2C, and 4C between 4.3 and 3.5 V at room temperature. The discharge profiles of singly substituted $LiMn_{2-y}M_yO_4$ (M = Li, Co, and Ni) and doubly substituted $LiMn_{2-y-z}Ni_yLi_zO_4$ samples are compared, respectively, in Figures 3 and 4 at various rates. The cation-substituted samples generally exhibit better rate capabilities than $LiMn_2O_4$. However, for the same degree of substitution, the doubly substituted samples show better rate capability than the singly substituted samples. For example, both $LiMn_{1.85}Ni_{0.075}Li_{0.075}O_4$ and $LiMn_{1.8}Ni_{0.1}Li_{0.1}O_4$ retain 98% of their discharge capacity on increasing the rate from C/10 to 4C. In contrast, $LiMn_2O_4$ and $LiMn_{1.85}Ni_{0.15}O_4$ retain only 47% and 86% of their discharge capacities, respectively, on going from C/10 to 4C rate. Furthermore, the doubly substituted $LiMn_{1.85}Ni_{0.075}Li_{0.075}O_4$ retains 84% and 57% of its capacity on increasing the rate from C/10 to 10C and 20C, respectively, as seen in Figure 5. The $LiMn_{1.85}Ni_{0.075}Li_{0.075}O_4$ sample regains its full capacity quickly on changing the rate from 10C or 20C to C/10 to 2C (Figure 5), illustrating that the cyclability is not degraded by drastic changes in the C rates. The remarkable rate capability of $LiMn_{1.85}Ni_{0.075}Li_{0.075}O_4$ coupled with the low cost and low toxicity, despite a slightly lower capacity (~100 mAh/g) than $LiMn_2O_4$, may make it attractive for electric vehicle applications.

Storage Characteristics. The storage performances were evaluated by subjecting the coin cells to one charge−discharge cycle at room temperature between 4.3 and 3.5 V followed by discharging to various depths of discharge (DOD) in the second cycle, storing at 60 °C for 7 d at various DOD, completing the second discharge cycle after cooling to ambient temperatures, and evaluating the full discharge capacity in the third cycle at room temperature. Figure 6 compares the % capacity retention after storing at various DOD for $LiMn_2O_4$, $LiMn_{1.85}Ni_{0.075}Li_{0.075}O_4$, and $LiMn_{1.8}Ni_{0.1}Li_{0.1}O_4$. The %

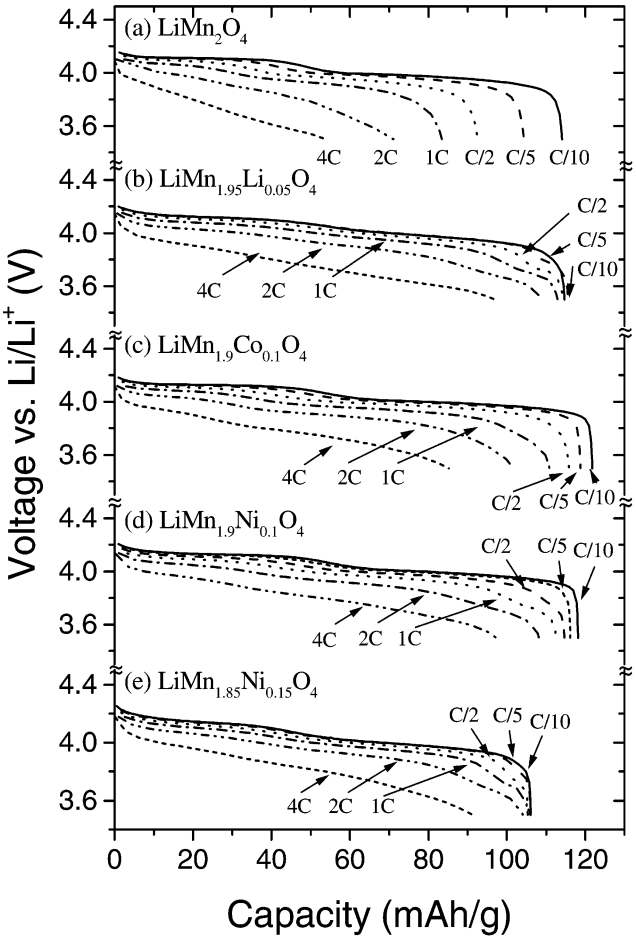

Figure 3. Comparison of the discharge profiles of singly substituted $LiMn_{2-y}M_yO_4$ (M = Li, Co, and Ni) samples with that of $LiMn_2O_4$ at C/10, C/5, C/2, 1C, 2C, and 4C rates, illustrating the rate capability.

capacity retention was obtained as a ratio of the third discharge capacity to the first discharge capacity. Although $LiMn_2O_4$ loses a significant amount of capacity after storage (10−40%), both $LiMn_{1.85}Ni_{0.075}Li_{0.075}O_4$ and $LiMn_{1.8}Ni_{0.1}Li_{0.1}O_4$ retain >95% of their initial capacity, illustrating excellent storage characteristics. The capacity retention of the $LiMn_2O_4$ system decreases with increasing DOD first, reaches a minimum around 60−80% DOD, and then increases, which is in agreement with the trend reported by others in the literature.[27]

Manganese Dissolution. The manganese dissolution was evaluated for various samples by two different procedures described in the Experimental Section. Figure 7 compares the variations of the amount of dissolved manganese on soaking in the electrolyte at 55 °C for 7 d with the % capacity loss found after 50 cycles at room temperature. The dissolved amount of manganese is in the range of 1.3−3% with considerable scatter in the data. The unsubstituted $LiMn_2O_4$ (sample 1) exhibiting the highest capacity loss in Table 1 shows lower manganese dissolution (1.8%) than several other cation-substituted samples that exhibit much better capacity retention. Moreover, the $LiCoO_2$ cathode, which is known to exhibit excellent electrochemical performance, also shows a comparable or significant amount of cobalt dissolution (0.7%) under similar conditions. These observations are in agreement with some of the literature data pointing out a lack of correlation between the amount of dissolved manganese and capacity retention.[4−6]

Figure 8 compares the variations of the amount of dissolved manganese found after washing the cycled (after 20 cycles at 60 °C) cell components (cathode, anode, and separator) with deionized water or propylene carbonate with the % capacity loss found after 20 cycles at 60 °C. The amount of dissolved manganese is slightly higher after soaking in propylene carbonate compared

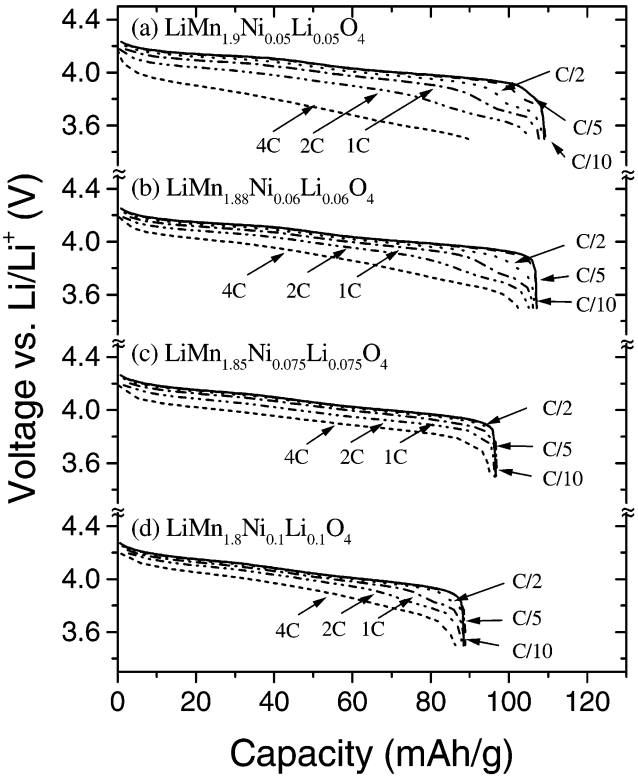

Figure 4. Discharge profiles of doubly substituted $LiMn_{2-y-z}Ni_yLi_zO_4$ samples at C/10, C/5, C/2, 1C, 2C, and 4C rates, illustrating the rate capability.

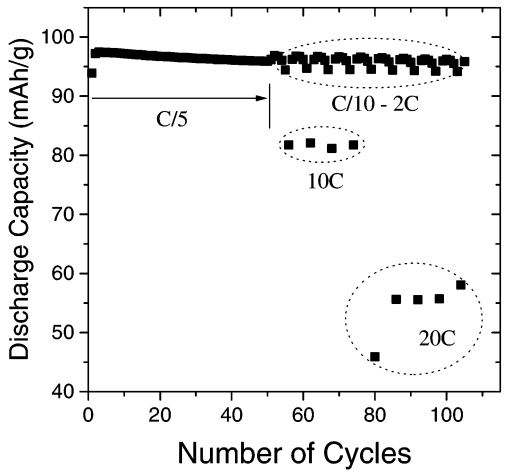

Figure 5. Cycling performance of $LiMn_{1.85}Ni_{0.075}Li_{0.075}O_4$ at various rates between C/10 and 20C at room temperature. In the region marked as C/10−2C, the data points with higher capacity values refer to C/10 rate and those with lower capacity values refer to 2C rate.

(27) Saito, T.; Machida, M.; Yamamoto, Y.; Nagamine, M. In *Electrochemical Society Meeting Abstracts, v. 2001-2;* Electrochemical Society: Pennington, NJ, 2001; p 180.

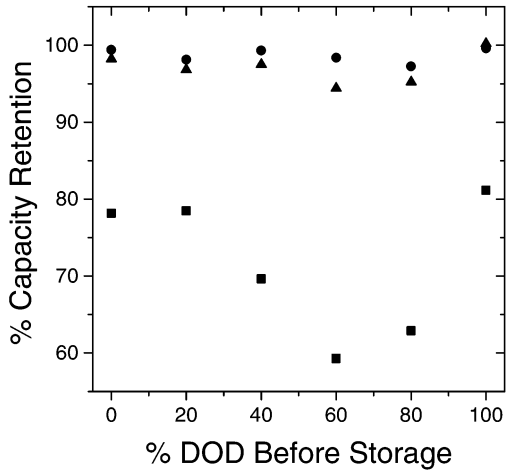

Figure 6. Comparison of the % capacity retention after storage at 60 °C for 7 d at different depth of discharge (DOD): (■) $LiMn_2O_4$; (●) $LiMn_{1.85}Ni_{0.075}Li_{0.075}O_4$; and (▲) $LiMn_{1.8}Ni_{0.1}Li_{0.1}O_4$.

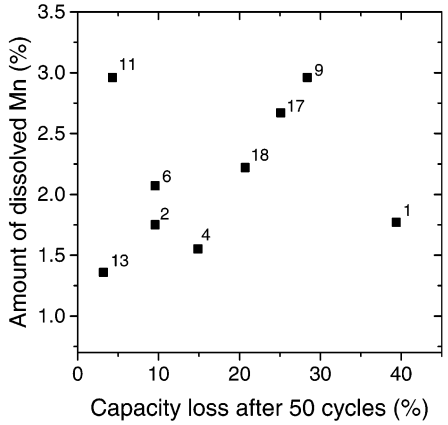

Figure 7. Relationship between the amount of dissolved manganese and the % capacity loss after 50 cycles at room temperature. The dissolved manganese was obtained by soaking the oxides in the electrolyte consisting of 1 M $LiPF_6$ in EC/DEC at 55 °C for 7 d. Numbers in the figure refer to sample numbers in Table 1.

to that after soaking in water. Although $LiMn_2O_4$ exhibiting the highest capacity loss shows the highest amount of dissolved manganese, the difference in manganese dissolution among the various samples is small to account for the drastic differences in the % capacity loss (41 to 3%). These observations suggest that manganese dissolution may not be the sole factor responsible for capacity fade in spinel manganese oxides.

Loss of Crystallinity and Microstrain. Figure 9 compares the X-ray diffraction patterns of $LiMn_2O_4$ with those of some doubly substituted $LiMn_{2-y-z}M_yLi_zO_4$ (M = Ti and Ni) after cycling. Although $LiMn_2O_4$ shows significant line broadening and loss of crystallinity after cycling at room temperature for 50 cycles (Figure 9b), both $LiMn_{1.85}Ni_{0.075}Li_{0.075}O_4$ and $LiMn_{1.8}Ni_{0.1}Li_{0.1}O_4$ maintain their crystallinity with sharp diffraction peaks even after cycling at 60 °C for 100 cycles (Figure 9c and d). Also, $LiMn_{1.85}Ti_{0.075}Li_{0.075}O_4$ exhibiting significant capacity loss (Table 1) shows line broadening after 100 cycles at room temperature (Figure 9e) although less than that found with $LiMn_2O_4$ (Figure 9b). The data reveal that the samples exhibiting good cyclability

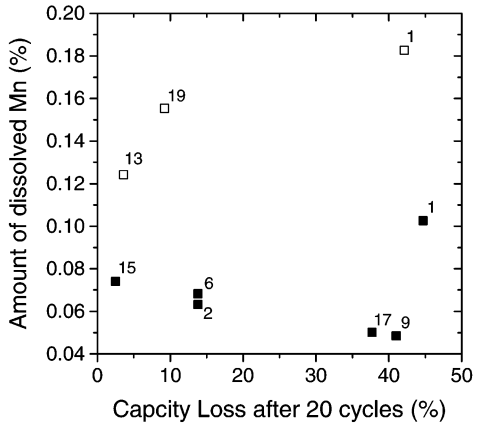

Figure 8. Relationship between the amount of dissolved manganese and the % capacity loss after 20 cycles at 60 °C. The dissolved manganese was obtained by washing the coin cell components (cathode, anode, and separator) with deionized water (■) or propylene carbonate (□) after 20 cycles at 60 °C. Numbers in the figure refer to the sample numbers in Table 1.

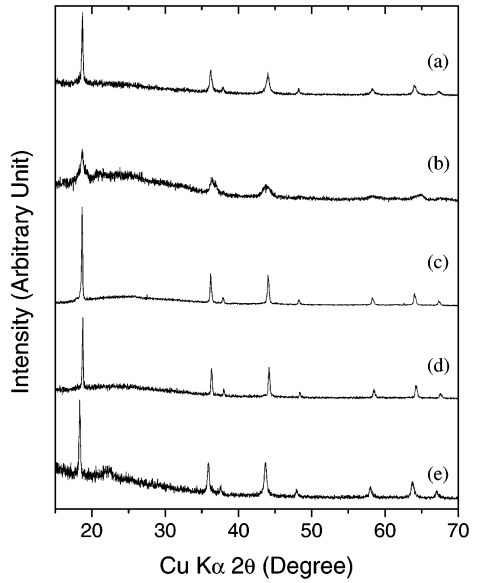

Figure 9. X-ray diffraction patterns of $LiMn_{2-y-z}M_yLi_zO_4$ spinel oxides after cycling: (a) $LiMn_2O_4$ after 1 cycle at room temperature; (b) $LiMn_2O_4$ after 50 cycles at room temperature; (c) $LiMn_{1.85}Ni_{0.075}Li_{0.075}O_4$ after 100 cycles at 60 °C; (d) $LiMn_{1.8}Ni_{0.1}Li_{0.1}O_4$ after 100 cycles at 60 °C; and (e) $LiMn_{1.85}Ti_{0.075}Li_{0.075}O_4$ after 100 cycles at room temperature.

maintain their crystallinity with sharp diffraction peaks after cycling.

In general, several factors can contribute to the broadening of peaks in X-ray diffraction.[28−30] For example, instrumental factors related to the resolution and the incident X-ray wavelength, as well as sample factors such as crystallite size and nonuniform microstrain, can cause line broadening. In the case of instrumental broadening, line widths will vary smoothly with 2θ or d spacing. On the other hand, line broadening originating from sample characteristics will have a

(28) Young, R. A. *The Rietveld Method*; Oxford University Press: New York, 1993.
(29) Cullity, B. D. *Elements of X-ray Diffraction*; Addison-Wesley: Reading, MA, 1978.
(30) Hammond, C. *The Basics of Crystallography and Diffraction*; Oxford University Press: New York, 1997.

Table 2. X-ray Diffraction Analysis Results of $Li_{1-x}Mn_{2-y-z}M_yLi_zO_4$

	as-prepared[a]			after treating with acid				after chemically extracting lithium			
composition	lattice param. (Å)	crystal. size (Å)	strain (%)	Li content $(1-x)$	lattice param. (Å)	crystal. size (Å)	strain (%)	Li content $(1-x)$	lattice param. (Å)	crystal. size (Å)	strain (%)
$Li_{1-x}Mn_2O_4$	8.246	1229	0.0155	0.00	8.032	1250	0.1691	0.12	8.044	581	0.1405
$Li_{1-x}Mn_{1.9}Co_{0.1}O_4$	8.232	749	0.0084	0.10	8.038	665	0.0162	0.17	8.043	918	0.0771
$Li_{1-x}Mn_{1.9}Ni_{0.1}O_4$	8.236	574	0.0000	0.14	8.048	758	0.0175	0.20	8.059	729	0.0675
$Li_{1-x}Mn_{1.95}Li_{0.05}O_4$	8.231	626	0.0000	0.12	8.056	935	0.0412	0.18	8.050	940	0.0874
$Li_{1-x}Mn_{1.9}Co_{0.05}Li_{0.05}O_4$	8.221	794	0.0093	0.20	8.049	864	0.0166	0.21	8.052	986	0.0506
$Li_{1-x}Mn_{1.9}Ni_{0.05}Li_{0.05}O_4$	8.218	664	0.0110	0.24	8.067	1015	0.0284	0.22	8.060	776	0.0205
$Li_{1-x}Mn_{1.8}Ni_{0.1}Li_{0.1}O_4$	8.202	747	0.0695	0.41	8.079	713	0.0806	0.41	8.084	521	0.0633

[a] All the as-prepared samples had a lithium content $(1-x)$ of 1.00.

different relationship. For example, by combining the Scherrer's equation for crystallite size effect and Bragg's law for diffraction, a relationship between full width at half-maximum (fwhm) and diffraction angle can be derived as[16]

$$\beta \cos\theta = {}^{\lambda}/_{\tau} + k\epsilon \sin\theta \qquad (1)$$

where β is the fwhm, θ is the diffraction angle, λ is the incident X-ray wavelength, τ is the crystallite size, k is a constant, and ϵ is the microstrain $\delta d/d$ (d is interplanar spacing). The crystallite size and strain effects can be separated by plotting fwhm multiplied by cos θ vs. sin θ, in which the slope $k\epsilon$ will be related to the microstrain and the intercept ${}^{\lambda}/_{\tau}$ will be related to the crystallite size.

Crystallite size and strain analyses of the various spinel manganese oxides were performed by the JADE software before and after soaking the samples in the electrolyte at 55 °C for 7 d and chemically extracting lithium with acid or NO_2BF_4 at room temperature, and the results are given in Table 2 and Figure 10. In Figure 10, the slope is related to the strain and the intercept is related to the crystallite size. For both $LiMn_2O_4$ and the cation-substituted samples, the intercepts have similar values before and after soaking in the electrolyte or lithium extraction, indicating that the crystallite size does not change significantly during the chemical treatments. On the other hand, the slope of $LiMn_2O_4$ becomes steeper after the treatments compared to that before the treatments, suggesting that the $LiMn_2O_4$ system experiences a large amount of microstrain during lithium extraction (charging). In contrast, the cation-substituted samples in Figure 10 exhibit nearly the same or only a slight increase in slope after the treatments, suggesting little or a lower degree of microstrain. The magnitude of microstrain in Table 2 correlates with the % capacity loss in Table 1. As the magnitude of microstrain decreases, the % capacity loss decreases. It is interesting to note that for the same degree of cationic substitution, the doubly substituted samples such as $LiMn_{1.9}Ni_{0.05}Li_{0.05}O_4$ exhibit lower microstrain compared to the singly substituted samples such as $LiMn_{1.9}Ni_{0.1}O_4$. Accordingly, the doubly substituted samples exhibit superior capacity retention and rate capability compared to those of the singly substituted samples. Thus, although manganese dissolution is definitely a problem, the development of microstrain appears to be more important in the capacity fading of spinel manganese oxides.[4,14,16,23]

Lattice Parameter Differences between the Two Cubic Phases and Microstrain. To understand the origin of microstrain, we have focused on the cubic to cubic phase transition and the two-phase region that occur in the 4 V region of $LiMn_2O_4$ spinel. The two-phase region in $LiMn_2O_4$ has been suggested to introduce instability, particularly at elevated temperatures,[15] and cation-substituted samples such as $Li_{1.05}Mn_{1.95}O_4$ have been shown to experience a smaller lattice parameter difference in the two-phase region compared to that of $LiMn_2O_4$.[31] To assess the influence of the two-phase region, we have examined the evolution of the X-ray diffraction patterns with lithium content and the lattice parameter difference between the two cubic phases that exist in the 4 V region.

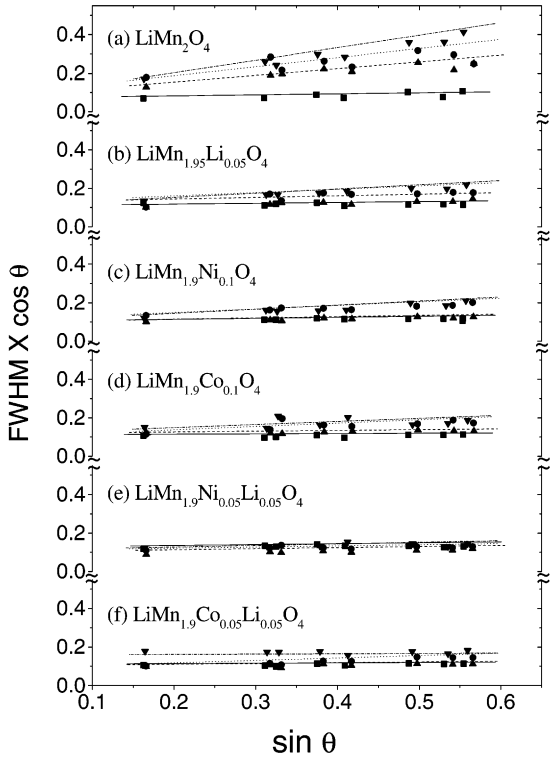

Figure 10. Crystallite size and strain analyses of $Li_{1-x}Mn_{2-y-z}M_yLi_zO_4$ spinel oxides: (■) as-prepared samples before chemical treatment; (●) after extracting lithium with acid; (▲) after extracting lithium with NO_2BF_4; and (▼) after soaking with the electrolyte at 55 °C for 7 days.

Figure 11 compares the evolution of the X-ray diffraction patterns of $Li_{1-x}Mn_2O_4$, $Li_{1-x}Mn_{1.9}Co_{0.1}O_4$, and $Li_{1-x}Mn_{1.9}Ni_{0.05}Li_{0.05}O_4$ that were obtained by chemically extracting lithium with NO_2BF_4. The splitting of the

(31) Sun, X.; Yang, X. Q.; Balasubramanian, M.; McBreen, J.; Xia, Y.; Sakai, T. *J. Electrochem. Soc.* **2002**, *149*, A842.

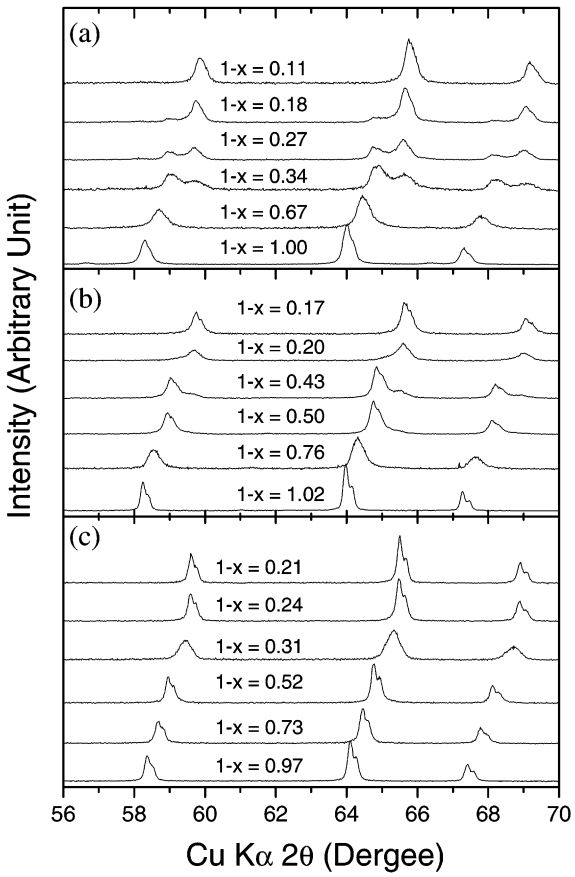

Figure 11. X-ray diffraction patterns of the (a) $Li_{1-x}Mn_2O_4$, (b) $Li_{1-x}Mn_{1.9}Co_{0.1}O_4$, and (c) $Li_{1-x}Mn_{1.9}Ni_{0.05}Li_{0.05}O_4$ samples that were obtained by chemically extracting lithium with NO_2-BF_4.

reflections into two distinct peaks as in the cases of $Li_{1-x}Mn_2O_4$ and $Li_{1-x}Mn_{1.9}Co_{0.1}O_4$ or the occurrence of broad reflections as in the case of $Li_{1-x}Mn_{1.9}Ni_{0.05}Li_{0.05}O_4$ around $(1 - x) \approx 0.3-0.5$ is due to the presence of two cubic phases. Figure 12 compares the X-ray diffraction patterns of several compositions in the two-phase region. Whereas $Li_{1-x}Mn_2O_4$ and the singly substituted samples such as $Li_{1-x}Mn_{1.9}M_{0.1}O_4$ (M = Co and Ni) show two well-separated, distinct peaks corresponding to the two cubic phases that have a larger difference in lattice parameters, the doubly substituted samples such as $Li_{1-x}Mn_{1.9}M_{0.05}Li_{0.05}O_4$ (M = Co and Ni) show only broad peaks without a clear splitting due to close lattice parameters for the two phases.

Despite the broad peaks for the $Li_{1-x}Mn_{2-y-z}M_yLi_zO_4$ samples in the two-phase region, the reflections could be resolved by Rietveld refinement to obtain the lattice parameters for the two cubic phases. Figure 13 relates the lattice parameter difference, Δa, between the two cubic phases as well as the corresponding % volume change, ΔV, (Table 1) to the % capacity fade for several samples investigated in this study. The Δa values change slightly with the lithium content within the two-phase region, and the maximum value of Δa found in the two-phase region is used in Figure 13. For comparison, Figure 13 also plots the lattice parameter difference, $\Delta a'$, between the fully discharged and charged states vs the % capacity fade. As seen in Figure 13, Δa and the corresponding ΔV show a better linear relationship with the % capacity fade than $\Delta a'$. The smaller the

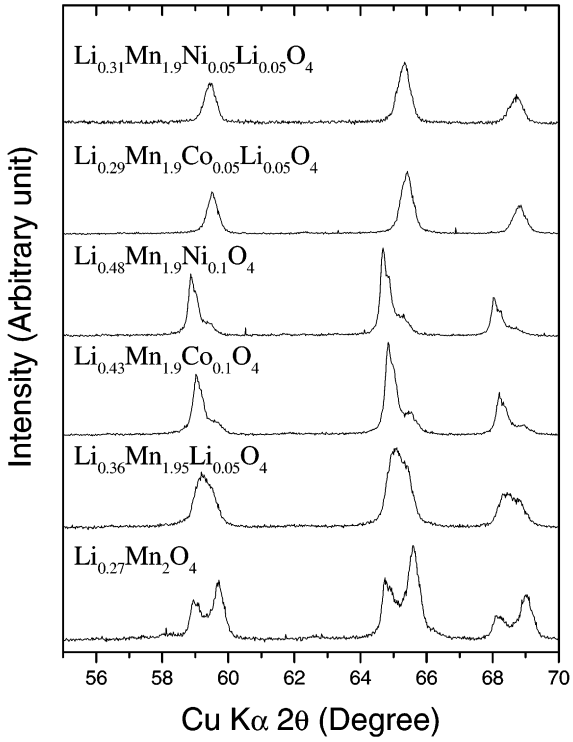

Figure 12. X-ray diffraction patterns of the $Li_{1-x}Mn_{2-y-z}M_yLi_zO_4$ samples in the two-phase region consisting of two cubic phases. The samples were obtained by chemically extracting lithium with NO_2BF_4.

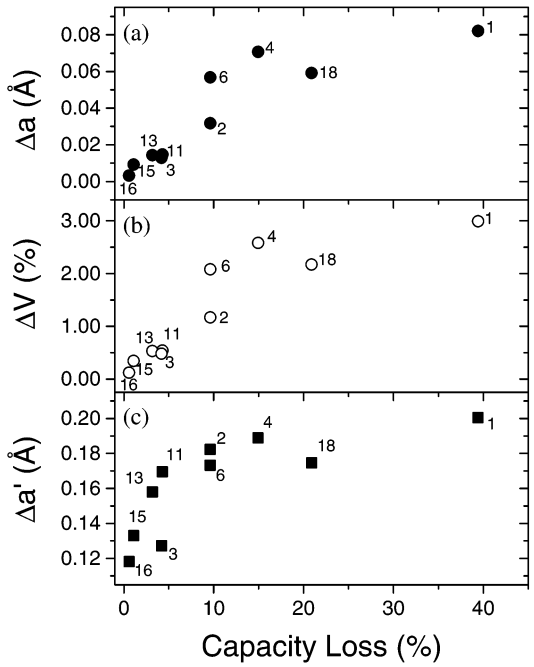

Figure 13. Correlation of the lattice parameter differences (Δa and $\Delta a'$) and the volume change ΔV with the % capacity loss found after 50 cycles at room temperature: Δa is the maximum difference in lattice parameters between the two cubic phases formed at $(1 - x) \approx 0.3-0.5$ in $Li_{1-x}Mn_{2-y-z}M_yLi_zO_4$; ΔV is the corresponding volume change calculated from Δa; and $\Delta a'$ is the difference in lattice parameters between the fully discharged and charged states of $Li_{1-x}Mn_{2-y-z}M_yLi_zO_4$. Numbers in the figure correspond to the sample numbers in Table 1.

values of Δa and ΔV, the lower are the microstrain and % capacity fade or the better is the capacity retention.

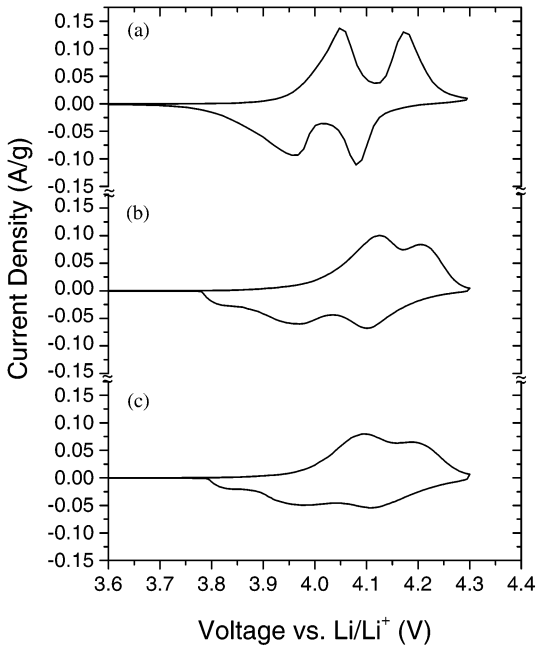

Figure 14. Comparison of the cyclic voltammograms of (a) $LiMn_2O_4$, (b) $LiMn_{1.85}Ni_{0.15}O_4$, and (c) $LiMn_{1.85}Ni_{0.075}Li_{0.075}O_4$ between 3.6 and 4.3 V at a scan rate of 50 μV/s.

$LiMn_2O_4$, with the largest value of Δa and ΔV, shows the highest % capacity fade and microstrain. A large instantaneous volume change (3% in $LiMn_2O_4$) on going from one cubic phase to another cubic phase can lead to a loss of interparticle contact and breaking of particles during the discharge−charge cycling, resulting in poor Li^+ diffusion, electrical conductivity, and capacity retention. It can be considered analogous to the instantaneous volume change (5.6%) occurring during Jahn−Teller distortion in the 3 V region of $LiMn_2O_4$.[29] The instantaneous volume changes can also lead to the formation of new surfaces, enhancing the electrode−electrolyte reactivity.

Figure 14 compares cyclic voltammograms (CV) of some spinel manganese oxides. Whereas the two plateaus occurring in the 4 V region (one around 3.9 V and the other around 4.1 V) could be clearly visualized in $LiMn_2O_4$ and in the singly substituted samples (Figure 3), it becomes more difficult to distinguish the two plateaus in some doubly substituted samples such as $LiMn_{1.85}Ni_{0.075}Li_{0.075}O_4$ (Figure 4c). However, all the cation-substituted (both singly and doubly substituted) samples show two redox peaks around 3.9 and 4.1 V similar to $LiMn_2O_4$ in the CV (Figure 14) although the resolution between the peaks is suppressed in the cation-substituted samples. The CV data confirm the formation of two cubic phases in all the samples despite the smaller lattice parameter differences and broad diffraction peaks in some cases such as $LiMn_{1.85}Ni_{0.075}Li_{0.075}O_4$.

Conclusions

A cosubstitution of small amounts of Li and Ni for Mn in the spinel lithium manganese oxide $LiMn_{2-y-z}Ni_yLi_zO_4$ ($0.05 \leq y \leq 0.1$ and $0.05 \leq z \leq 0.1$) has been found to improve the electrochemical performances significantly. The $LiMn_{2-y-z}Ni_yLi_zO_4$ samples exhibit superior cyclability at elevated temperatures, high rate capability, and excellent capacity retention after storage at 60 °C for extended periods of time at various DOD, with moderate reversible capacities of around 100 mAh/g compared to $LiMn_2O_4$ although the degree of manganese dissolution does not vary significantly. The superior electrochemical properties of $LiMn_{2-y-z}Ni_yLi_zO_4$ are found to be due to a smaller lattice parameter difference between the two cubic phases formed in the 4 V region. The smaller or negligible instantaneous volume changes appear to suppress the microstrain and impart superior electrochemical properties. The excellent performance, as well as the low cost, low toxicity, and easy synthesis, of the $LiMn_{2-y-z}Ni_yLi_zO_4$ cathodes may make them attractive for high-power applications such as electric vehicles. Furthermore, use of the concept of minimizing the lattice parameter differences between the two cubic phases may lead to the design and development of new cathode compositions based on spinel manganese oxides.

Acknowledgment. Financial support by the NASA Glenn Research Center and the Welch Foundation Grant F-1254 is gratefully acknowledged.

CM0341787